RESEARCH

Open Access

Establishment and characterization of patient-derived head and neck cancer models from surgical specimens and endoscopic biopsies

Daniel Strüder[1], Theresa Momper[2], Nina Irmscher[2], Mareike Krause[2], Jan Liese[3], Sebastian Schraven[1], Annette Zimpfer[4], Sarah Zonnur[4], Ann-Sophie Burmeister[2], Björn Schneider[4], Bernhard Frerich[3], Robert Mlynski[1], Christina Große-Thie[2], Christian Junghanss[2] and Claudia Maletzki[2]*

Abstract

Background: Head and neck squamous cell carcinoma (HNSCC) is heterogeneous in etiology, phenotype and biology. Patient-derived xenografts (PDX) maintain morphology and molecular profiling of the original tumors and have become a standard "Avatar" model for human cancer research. However, restricted availability of tumor samples hindered the widespread use of PDX. Most PDX-projects include only surgical specimens because reliable engraftment from biopsies is missing. Therefore, sample collection is limited and excludes recurrent and metastatic, non-resectable cancer from preclinical models as well as future personalized medicine.

Methods: This study compares the PDX-take rate, -growth, histopathology, and molecular characteristics of endoscopic specimens with surgical specimens. HNSCC samples ($n = 55$) were collected ad hoc, fresh frozen and implanted into NOD.Cg-Prkdc^{scid}Il2rg^{tm1Wjl}/SzJ mice.

Results: Engraftment was successful in both sample types. However, engraftment rate was lower (21 *vs.* 52%) and growth delayed (11.2 *vs.* 6.7 weeks) for endoscopic biopsies. Following engraftment, growth kinetic was similar. Comparisons of primary tumors and corresponding PDX models confirmed preservation of histomorphology (HE histology) and molecular profile (Illumina Cancer Hotspot Panel) of the patients' tumors. Accompanying flow cytometry on primary tumor specimens revealed a heterogeneous tumor microenvironment among individual cases and identified M2-like macrophages as positive predictors for engraftment. Vice versa, a high PD-L1 expression (combined positive score on tumor/immune cells) predicted PDX rejection.

Conclusion: Including biopsy samples from locally advanced or metastatic lesions from patients with non-surgical treatment strategies, increases the availability of PDX for basic and translational research. This facilitates (pre-) clinical studies for individual response prediction based on immunological biomarkers.

Keywords: Primary cancer, HPV positive and negative, Individual tumor models, Immune cell infiltration, Recurrence, Metastasis, Non-resectable, Endoscopic biopsy, Head and neck squamous cell carcinoma

*Correspondence: claudia.maletzki@med.uni-rostock.de
[2] Department of Internal Medicine, Medical Clinic III - Hematology, Oncology, Palliative Medicine, Rostock University Medical Center, Schillingallee 70, 18057 Rostock, Germany
Full list of author information is available at the end of the article

Strüder *et al. Journal of Experimental & Clinical Cancer Research*   (2021) 40:246

Page 2 of 13

Background

Head and neck squamous cell cancer (HNSCC) is the 7th most common cancer worldwide and associated with a poor outcome [1–5]. Despite aggressive surgery, radiation- and chemotherapy, ~ 50% of patients die, while survivors suffer from pain, dysphagia and dysphonia [6]. Today, recurrence, and treatment response are difficult to predict, because of inter- and intratumoral heterogeneity in etiology, phenotype, and biology. Preclinical models must represent this heterogeneity to identify predictive biomarkers and develop effective personalized medicine.

Patient-derived xenografts (PDX), generated by implantation of human cancer tissue into immunodeficient mice, are considered as the gold standard for preclinical cancer research [7–11]. In early passages, PDXs faithfully recapitulate the original tumors' cellular, molecular and histopathological structures as well as drug response and clinical outcome [8, 12]. Thus, PDX provide an excellent platform for translational research on biomarkers and drug development (including setup of clinical trials) [12–15].

However, the restricted availability of tumor samples hinders widespread use of PDX in HNSCC. The PDX take rate for surgical HNSCC-specimens (50–75%) is comparable to other solid tumors (lung ~ 30–60%, CRC 70%, pancreas ~ 50%) [14–21], but the availability of suitable specimens is limited. In early stage tumors, the pathologist needs most of the surgery specimen for tumor staging and margin controls, while advanced (metastatic) disease is mostly treated with chemo-, immune- or radiation therapy (without surgery). Therefore, PDX from surgery specimens exclude recurrent and advanced (metastatic) HNSCC from preclinical models and personalized medicine.

In lung-, gastrointestinal-, pancreatic-, bladder- and skin cancer PDX-projects, the lack of surgical specimens has led to the use of endoscopic- and needle biopsies [15, 22, 23]. Engraftment rates were lower for biopsies (33–60%) *vs.* surgery specimens (40–100%), but PDX formation from minimally invasive procedures was possible. For HNSCC, endoscopic PDX sampling appears technically suitable, because of exophytic tumor growth and diagnostic sampling from both the vital margin and the necrotic center of the lesion. Two recent HNSCC studies regularly used biopsies for PDX formation [24, 25]. Lilja-Fischer et al. reported a biopsy take rate of 33% in oropharyngeal cancer [24] while Kang et al. observed 100% engraftment efficacy for biopsies in a small and defined patient cohort [26]. Therefore, HNSCC PDX biopsy engraftment appears to be feasible. However, take rate, time to engraftment and contributing factors of endoscopic biopsies for HNSCC PDX formation remain unclear.

In this study, we describe a practical and straightforward method to establish p16 positive and negative PDX models using endoscopic and surgical tumor samples. Performing a side-by-side comparison, we show that the engraftment rate was lower for biopsies, but PDX had similar growth kinetics once established. With this setup, a PDX library was created including clinical characteristics, pathological analysis as well as molecular and immunological data of the tumor microenvironment.
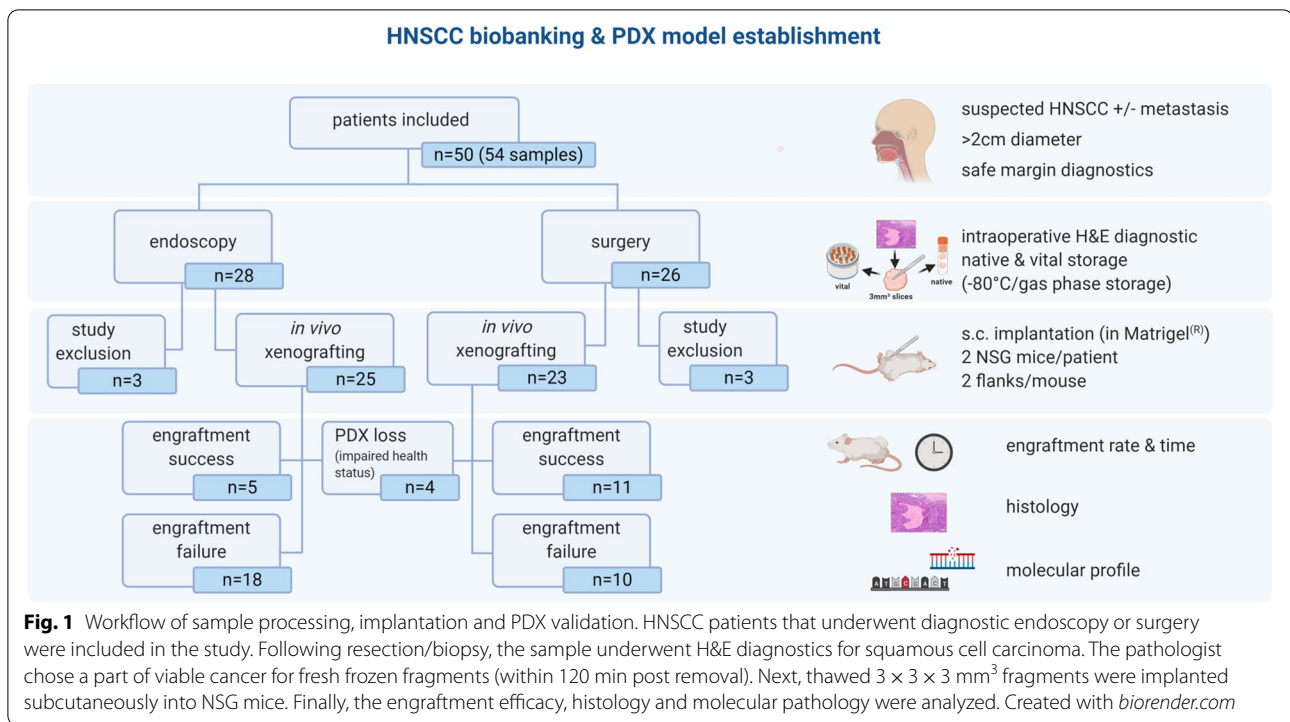
Materials and methods

Tumor sample preparation

HNSCC samples were donated from consecutive patients undergoing an endoscopic biopsy or surgery at a University Medical Center from 06/2018 through 01/2020. Patients with pathologically proven or suspicion of HNSCC and the following characteristics were eligible: 1) HNSCC of the oral cavity, oropharynx, hypopharynx, larynx and neck lymph node metastases; 2) size of the tumor > 2 cm; 3) primary disease or recurrence; 4) > 18 years of age. Written informed consent was obtained according to the local Ethics Committee (reference number A2018-0003) and the guidelines for the use of human material. Blood sampling (2×7.5 ml Heparin) was performed prior to endoscopy/surgery. Endoscopic biopsies were sampled using endoscopic scissors as required for the routine diagnostic procedure. Surgery specimens were obtained by open (e.g. pharyngotomy, laryngectomy) or transoral approach (e.g. laser, radio frequency).

Immediately after dissection, the samples were sent to the Institute of Pathology (in room temperature NaCl 0.9%) for instantaneous H&E section. The pathologist removed tumor tissue for routine diagnostics, necrotic/fibrotic areas and provided macroscopically vital tumor tissue for the experimental laboratory. All specimens of at least $5 \times 5 \times 5$ mm^3 were accepted and processed within 120 min of ischemia time using a clean bench. Tumor samples were cut into fragments of $3 \times 3 \times 3$ mm^3 and split: Two pieces were snap frozen and stored in liquid nitrogen for molecular analysis. The remaining fragments were frozen viable (FCS, 10% DMSO) and stored at -80 °C for xenografting (Fig. 1).

Ethical statement

All animal experiments were approved by the local governmental authority (approval number: 7221.3-1-066/18), in accordance with the governmental animal protection law and the EU Guideline 2010/63/EU. For in vivo engraftment, six-week-old female NOD.Cg-Prkdc^{scid}Il2rg^{tm1Wjl} (NSG, Charles River Laboratories, Lyon, France) mice were used as recipients. Mice were bred in the local animal core facility under specific pathogen-free

Fig. 1 Workflow of sample processing, implantation and PDX validation. HNSCC patients that underwent diagnostic endoscopy or surgery were included in the study. Following resection/biopsy, the sample underwent H&E diagnostics for squamous cell carcinoma. The pathologist chose a part of viable cancer for fresh frozen fragments (within 120 min post removal). Next, thawed $3 \times 3 \times 3$ mm^3 fragments were implanted subcutaneously into NSG mice. Finally, the engraftment efficacy, histology and molecular pathology were analyzed. Created with *biorender.com*

conditions. During the experiment, mice were kept in type III cages (Zoonlab GmbH, Castrop-Rauxel, Germany) at 12-h dark:light cycle, the temperature of 21 ± 2 °C, and relative humidity of $60 \pm 20\%$ with food (pellets, 10 mm, ssniff-Spezialdiäten GmbH, Soest, Germany) and tap water ad libitum. During their whole life-time, all animals received enrichment as mouse-igloos (ANT Tierhaltungsbedarf, Buxtehude, Germany), nesting material (shredded tissue paper, Verbandmittel GmbH, Frankenberg, Deutschland, paper roles (75×38 mm, H 0528–151, ssniff-Spezialdiäten GmbH), and wooden sticks ($40 \times 16 \times 10$ mm, Abedd, Vienna, Austria).

PDX generation
After melting of the frozen samples, DMSO was removed and the tumor fragments were embedded in Matrigel (Corning® Matrigel® Basement Membrane Matrix, Wiesbaden, Germany) for 10 min. Meanwhile, the NSG-mice were anesthetized using Ketamin/Xylazin (dose: 90/6 mg/kg bw). After verification of sufficient anesthesia, both hind flanks were shaved, iodine disinfected and incised (3 mm). Tumor fragments were implanted subcutaneously and wounds were closed using simple interrupted sutures (Ethicon 6–0, Johnson & Johnson GmbH, Neuss, Germany) followed by iodine disinfection. Mice were placed under a heating lamp during recovery from anaesthesia and received analgesia (Metamizol 1250 mg/l, in drinking water) (pre- and) post-surgery to reduce pain.

After recovery, the flank tumors were measured weekly using a caliper. If no tumor growth occurred for 6 months, mice were euthanized. When flank tumors grew and reached a maximum size of $1.5 \times 1.5 \times 1.5$ cm^3, euthanasia and tissue collection was performed. The tumor was minced as described for the primary sample. Briefly, two fragments were used for molecular and histological analysis and the remaining fragments were viable frozen for further passaging. Tumor nomenclature was as followed: HNSCC [serial number] P [passage P0/P1] M [mouse M1/M2]. The patients' serial numbers are maintained throughout all PDX passages.

Histology and immunohistochemistry of patient tumor tissue and PDX
Morphology of patient tumor tissue and their corresponding PDX models was studied by an expert pathologist. Histopathology of primary tumors and PDX followed standard protocols for HNSCC staging including HE staining and immunohistochemistry; antibodies: anti-CD8 (Clone C8/144B, Dako, Hamburg, Germany, anti-p16 (clone: G175-405, BD Bioscience, Heidelberg, Germany), anti-Ki-67 (Clone Mib-1, Dako), anti-PD-L1 (Clone 22C3, Dako).

Molecular pathology
Nucleic acids and proteins were isolated from snap frozen primary tumors and PDX [mean weight: 16.6 mg].

Simultaneous purification of DNA, RNA, and protein (from the same tissue sample) was performed using AllPrep DNA/RNA/Protein Mini Kit (Qiagen, Hilden, Germany) Isolation was executed according to the manufacturers' instructions: (I) tissue disruption and homogenization; (II) RNA isolation; (III) protein isolation; and (IV) gDNA isolation. Isolated nucleic acids and proteins were stored at -80 °C. gDNA samples were used to detect genomic alterations using the Illumina Cancer Hotspot Panel (Illumina, Berlin, Germany) covering mutations in 50 different genes with an iSeq100 sequencing system (Illumina) according to the manufacturer's protocols. For human papilloma virus (HPV) testing, a commercially available kit was used (VisionArray HPV Chip 1.0, Zyto-Vision, Bremerhaven, Germany) and applied according to the manufacturer's instructions.

Multi-color flow cytometry
Surface marker expression on single tumor cell suspensions was assessed by multi-color flow using a panel of human-specific conjugated antibodies (mAb, 1 µg each): anti-CD3 FITC (clone OKT-3), anti-CD4 PE (clone IT4), anti-CD8 PE (clone MEM-31), anti-CD56 PE (clone MEM-188), anti-CD16 APC (clone 3G8), anti-CD274 PECy7 (clone 29E.2A3), anti-CD70 FITC (clone 113–16), anti-CD14 FITC (clone 63D3), anti-CD204 PE (clone 7C9C20), anti-CD169 APC (clone 7–239), anti-CD163 PECy7 (clone GHI/61). Whole blood and tumor samples were stained for 30 min (4 °C). Afterwards, erythrocytes were lysed using 155 mM NH_4Cl (MERCK Millipore, Darmstadt, Germany), 10 mM $KHCO_3$ (MERCK Millipore), and 0.1 mM EDTA (Applichem, Darmstadt, Germany). Negative controls were stained with the appropriate isotypes (Biolegend) or left unstained. Cells were washed, resuspended in PBS and analyzed by flow cytometry on a FACSVerse Cytometer (BD Pharmingen). Data analysis was performed using BD FACSuite software (BD Pharmingen).

Statistics
Statistical evaluation was performed using GraphPad PRISM software, version 5.02 (GraphPad, San Diego, USA). Values are reported as the mean $\pm$ SD. After proving the assumption of normality, differences between biopsies and surgery specimens were calculated using the unpaired Student's t-test. If normality failed, the non-parametric Mann–Whitney U test was applied. Multiple comparisons were done using one way ANOVA on ranks (Bonferroni's Multiple Comparison Test). Spearman nonparametric correlation was used to calculate correlations between individual parameters (two-tailed P value). The criterion for significance was taken to be $p < 0.05$.

Results
Patient and sample characteristics
Fifty patients were included (male:female: 41:9) with high performance status (ECOG 1.06 ± 0.88) with a median age of 64.0 years (range 46 to 82) (Table 1 and Fig. 1). Most patients were smokers (68%, ≥ 10 py), without critical alcohol consumption (54%). The majority of patients presented with locally advanced disease (T4a/4b) and four with a recurrence after (chemo)-radiation. Tumors were localized in the oropharynx ($n = 19$), oral cavity ($n = 17$), larynx ($n = 11$) and hypopharynx ($n = 5$) (Table 1). Neck metastases were collected from four patients (primary + related metastasis: HNSCC40/40II/40III and HNSCC45/46; metastasis only: HNSCC08 and HNSCC48). One case was a HNSCC lymph node metastasis of unknown primary (CUP) (HNSCC37). Thirteen of the tumors were p16$^+$ (determined by p16 immunoreactivity, representative images of p16$^+$ and p16$^-$ cases are given in Fig. 2). To analyze whether p16 positivity is the result of HPV infection, molecular HPV testing was done (Supplementary Table 1). HPV was confirmed in 12 cases, whereas one case (HNSCC26) was finally classified as p16$^+$/HPV$^-$.

Table 1 Characteristics of the 50 study participants ($\Sigma = 56$ samples)

Group characteristics	Surgery $\Sigma n = 26$		Biopsy $\Sigma n = 28$	
	%	n	%	n
Female	15	4	18	5
Male	85	22	82	23
Age [years]	64.8	± 9.4	64.5	± 8.1
Performance status [ECOG]	1.0	± 0.7	1.1	± 1.0
Noxae				
Smoking [> 10 py]	73	19	68	19
Alcohol [> 1 drink/d]	58	15	32	9
Localization	38	10		
Oral cavity	23	6	25	7
Oropharnyx	12	3	46	13
Hypopharynx	27	7	7	2
Larynx			18	5
CUP			4	1
p16 status				
Positive	15	4	32	9
Negative	85	22	68	19
G1/G2/G3 [%]	6/73/21		5/70/25	
T1/T2/T3/T4 [%]	13/27/30/30		-/17/29/54*	
N0/N1/N2/N3 [%]	56/30/5/9		15/35/60/0*	

Values depict absolute/relative numbers and mean $\pm$ SD. Chi-square test was performed to analyze homogeneity of surgery *vs.* biopsy groups (*$p < 0.05$)

Abbreviations: *py* pack years, *CUP* cancer of unknown primary, *G1/2/3* grading
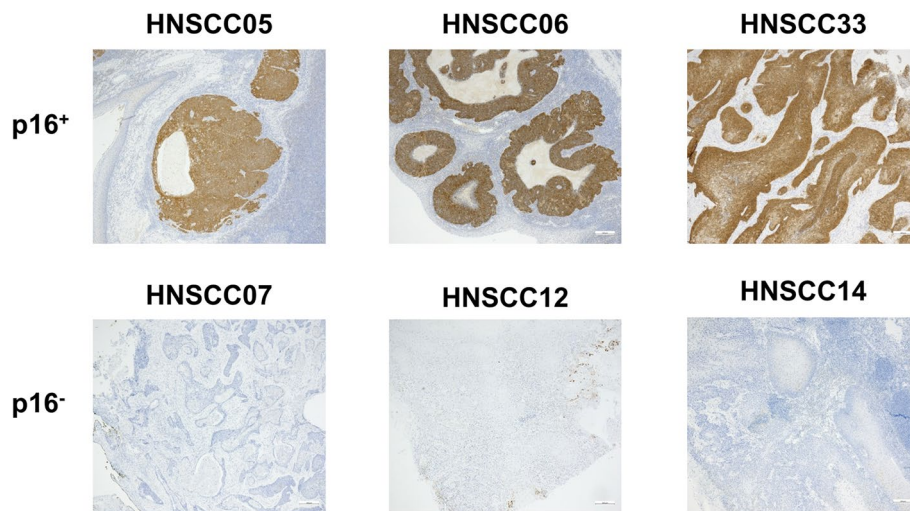
Fig. 2 Immunohistochemistry of p16. Representative images of p16$^+$ and p16$^−$ cases are shown (5 × magnification). Immunohistochemistry was done as described in material & methods using clone: G175-405

The mean sample size of the tumor piece was 1.2 ± 1.6 cm^3. In some cases of endoscopic biopsies, several pieces were obtained. Biopsy samples were smaller than surgical specimens (mean size: 0.9 cm^3 *vs.* 1.3 cm^3). The ischemia time was the same for biopsies and surgery samples (< 120 min, mean: 89.5 ± 33.6 min).

Detailed information on clinical follow-up, including adjuvant treatment, is summarized in Table 1. So far, four patients died because of progressive disease (HNSCC21, HNSCC31, HNSCC48, and HNSCC51).

PDX engraftment rate of biopsies and surgical specimens
Fourty eight cryopreserved individual HNSCC tumors were implanted subcutaneously into NSG mice (Table 1). Six HNSCC cases did not undergo PDX engraftment because of limitations in tumor quantity/quality and unspecific tumor type (CUP). Additional four HNSCC cases were lost because of impaired health of laboratory animals. Finally, 44 cases were included in data acquisition: 23 biopsy samples and 21 surgery samples.

Engraftment was obtained in 16 cases, yielding an overall efficacy of 36.4%. The engraftment rate was higher for surgical specimens (52.4 *vs.* 21.7%) and engraftment time was shorter (6.9 ± 2.4 *vs.* 10.6 ± 3.8 weeks; $p < 0.05$; Fig. 3A). After successful engraftment, PDX had comparable growth kinetics: Surgical specimens reached the maximum size in 9.5 ± 4.8 weeks and biopsies in 12.2 ± 4.6 weeks (Fig. 3A). Some aggressive cases grew in several flanks/implantation sites, while other cases did not engraft at all (Fig. 3B). Therefore, the positive flank related engraftment rate was 59.7% (Table 2). Again, the number of individual PDX/tumor was higher for surgical specimens (77.3%, Fig. 3B). Still, positive engraftment was seen in 37.5% of biopsy samples.

Notably, four PDX were established from p16$^+$/HPV-driven HNSCC cases (HNSCC06, HNSCC26, HNSCC42, and HNSCC54); three of them were taken from biopsies. Hence, the p16 status did not impact engraftment efficacy. Additional clinical parameters such as age, smoking, tumor localization, TNM stage and grade did not correlate with the engraftment. The same was true for the sampling related factors ischemia time and sample size (Table 3).

Serial passaging of the first seven established PDX models into P1 NSG mice was successful. All PDX grew after passaging and showed growth acceleration (time to tumor resection: 11.4 weeks vs. P0: 13.8 weeks) (Fig. 3C).

Histomorphology is preserved in PDX
All PDX closely resembled their primaries (Fig. 4). Tumor architecture, growth pattern, cytological features and stromal architecture were principally preserved. Besides, tumor differentiation (i.e., poor, moderate, or well) largely matched between patients and PDX models (Fig. 4). The PDX reflected intratumoral and intertumoral heterogeneity. Sometimes there were minor differences in tumor morphology (degree of keratinization) between individual mice: HNSCC13 P0 M1 showed strong keratinization, whereas in HNSCC13 P0 M2 the number of keratinizing areas was moderate (Fig. 5).

Regarding the biopsies and surgical specimens, no differences in preservation of morphology could be detected.
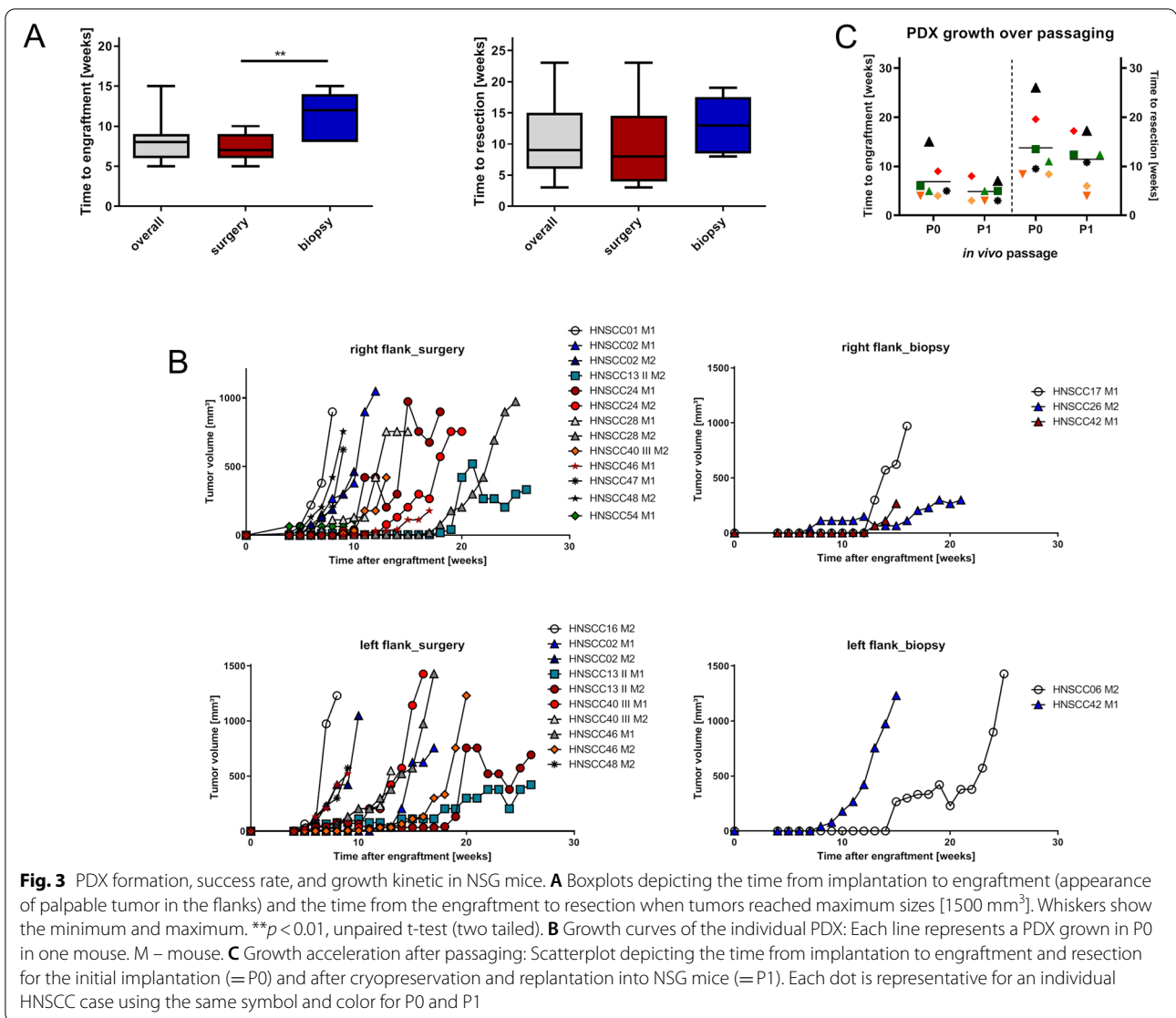
Fig. 3 PDX formation, success rate, and growth kinetic in NSG mice. **A** Boxplots depicting the time from implantation to engraftment (appearance of palpable tumor in the flanks) and the time from the engraftment to resection when tumors reached maximum sizes [1500 mm^3]. Whiskers show the minimum and maximum. **$p < 0.01$, unpaired t-test (two tailed). **B** Growth curves of the individual PDX: Each line represents a PDX grown in P0 in one mouse. M – mouse. **C** Growth acceleration after passaging: Scatterplot depicting the time from implantation to engraftment and resection for the initial implantation (= P0) and after cryopreservation and replantation into NSG mice (= P1). Each dot is representative for an individual HNSCC case using the same symbol and color for P0 and P1

Table 2 Overview on engraftment efficacy in NSG mice comparatively shown for biopsies and surgical specimen

Analyzed parameter	N	%
PDX engraftment [total]	16/44	36.36
Biopsies	5/23	21.73
Surgical resection specimen	11/21	52.38
Positive flanks [total]	43/72	59.72[a]
Biopsies	9/24	37.50[a]
Surgical resection specimen	34/44	77.30[a]

[a] taken from a total of two mice/case each implanted with two tumor fragments (left and right flank)

Table 3 Correlation analysis for PDX formation of HNSCC cases between biopsies and surgical specimen

Spearman correlation	*p* Value	Correlation coefficient[a]
Sample type	0.912	0.016
Sample size	0.300	-0.154
Age	0.887	0.021
Ischemia time	0.808	0.036
Ki-67 index	0.770	-0.043

[a] 1 = perfect positive correlation; -1 = perfect negative correlation; 0 = no correlation
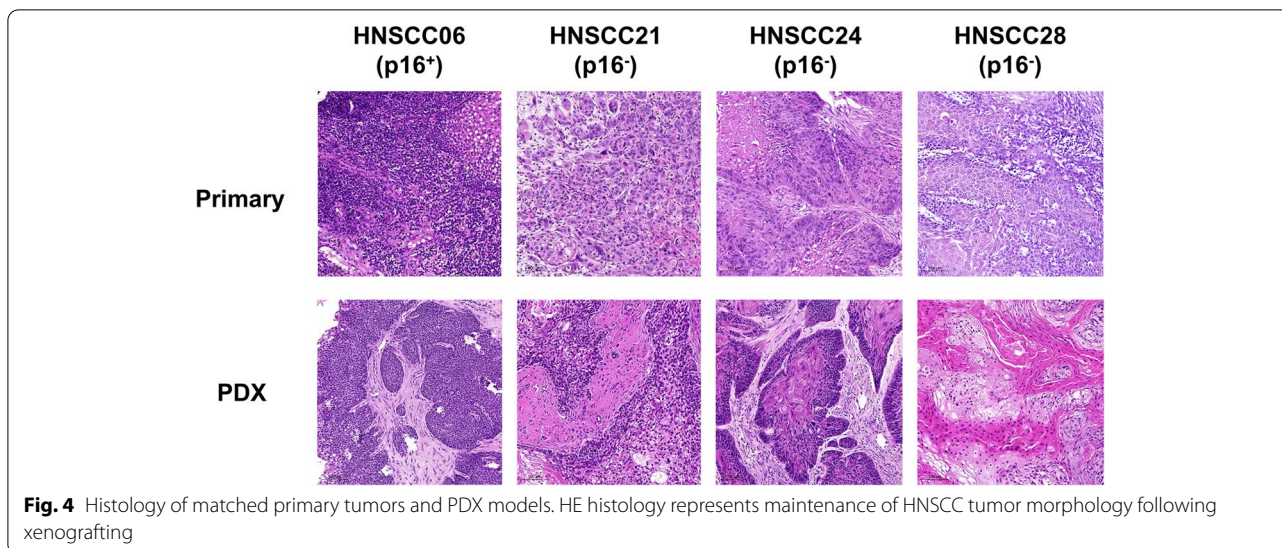
Fig. 4 Histology of matched primary tumors and PDX models. HE histology represents maintenance of HNSCC tumor morphology following xenografting
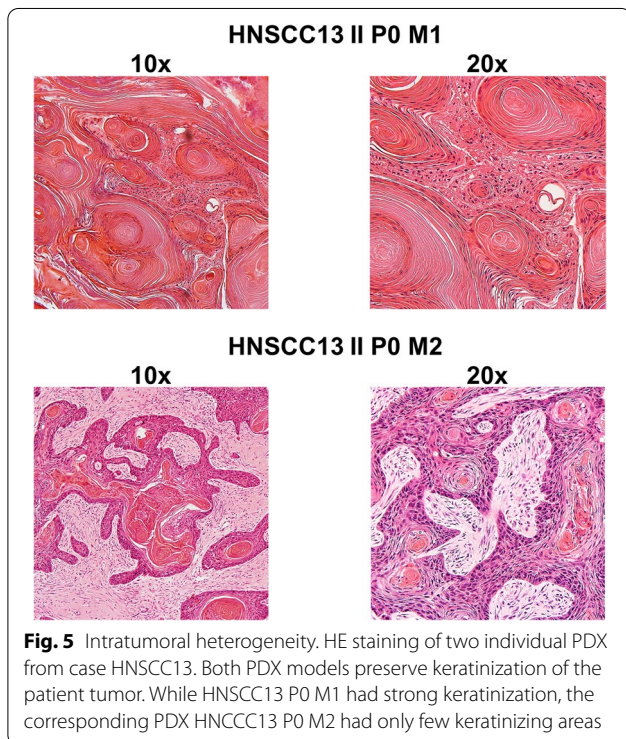

Fig. 5 Intratumoral heterogeneity. HE staining of two individual PDX from case HNSCC13. Both PDX models preserve keratinization of the patient tumor. While HNSCC13 P0 M1 had strong keratinization, the corresponding PDX HNCCC13 P0 M2 had only few keratinizing areas

Tumor microenvironment of patient tumors and PDX

Immunohistochemistry and flow cytometry revealed correlations between PDX engraftment, PD-L1 expression, and macrophage infiltration (Fig. 6). Immunohistological quantification of PD-L1 using the combined positive score (PD-L1 positivity in tumor and tumor-infiltrating immune cells), showed a trend towards better engraftment for low combined positive score (CPS $\leq$ 10); whereas c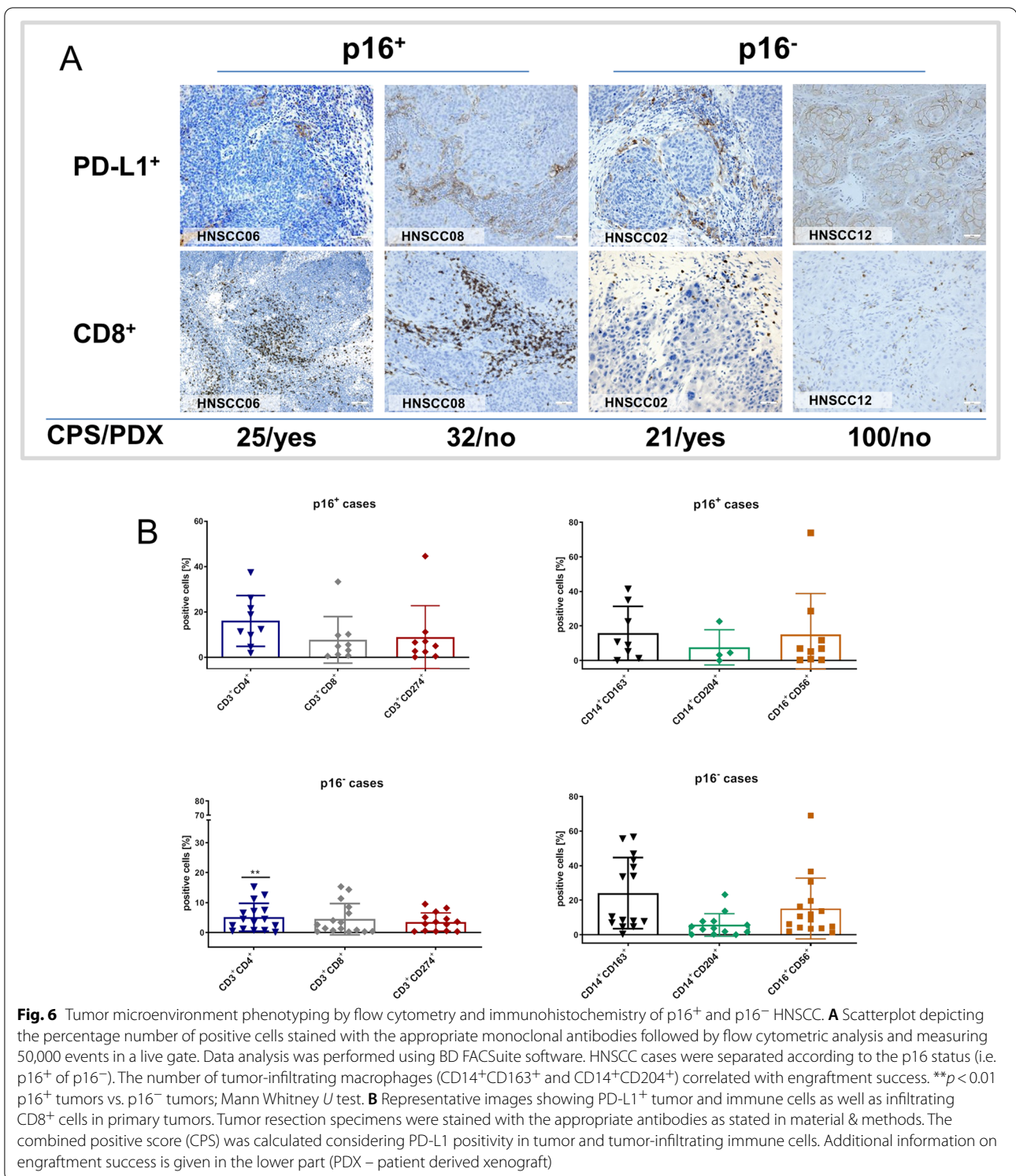ases with high CPS were more likely to be rejected (CPS [yes] *vs.* CPS [no]: 18.22 vs. 33.41; Pearson r: -0.109] (Fig. 6A).

The leukocyte infiltration of the tumor microenvironment was quantified by flow cytometry. Twenty five cases were analyzed (p16$^-$: 16 cases; p16$^+$: 9 cases). Leukocytic infiltration was heterogeneous (Fig. 6B), but p16$^+$ tumors showed a characteristic infiltration pattern. We identified high infiltration with CD3$^+$CD4$^+$ helper ($p < 0.01$ *vs.* p16$^-$ tumors) and CD3$^+$CD8$^+$ cytotoxic T cells, along with elevated numbers of CD3$^+$CD274$^+$ T cells. CD14$^+$CD163$^+$ and CD14$^+$CD204$^+$ macrophages were less frequent in p16$^+$ cases. CD16$^+$CD56$^+$ natural killer (NK) cells were heterogeneous irrespective of the p16 status.

Correlation of the innate immune cell compartment with PDX engraftment showed that engraftment was more frequent in cases with high numbers of CD14$^+$CD163$^+$ macrophages (Pearson r: -0.757; $p < 0.05$) and low numbers of CD14$^+$CD204$^+$ macrophages.

Molecular pathology is preserved in PDX

The mutational profile was studied in 13 patient samples and corresponding PDX. The overall number of genomic alterations in the cancer hotspot panel was low: *TP53* (61.5%) and *KDR* (38.4%) were the most affected genes. The direct comparison of the molecular fingerprint identified few discrepancies in most commonly affected genes (Fig. 7). In the PDX of HNSCC02, a *KRAS* mutation (c.114 T > C; variant allele frequency (VAF): 7.3%) and *SMARCB1* mutation (VAF: 5.2%) was detected. Vice versa, the patient tumor sample harbored an *EGFR* mutation (c.2361G > A; VAF: 30.5%) that was lost in the PDX. In HNSCC01, a *KRAS* mutation (c.114 T > C, VAF: 32.7%) was exclusively seen in the PDX. It can be assumed that intratumoral heterogeneity explains these findings best.

Strüder *et al. Journal of Experimental & Clinical Cancer Research*   (2021) 40:246

Page 8 of 13

Fig. 6 Tumor microenvironment phenotyping by flow cytometry and immunohistochemistry of p16+ and p16− HNSCC. **A** Scatterplot depicting the percentage number of positive cells stained with the appropriate monoclonal antibodies followed by flow cytometric analysis and measuring 50,000 events in a live gate. Data analysis was performed using BD FACSuite software. HNSCC cases were separated according to the p16 status (i.e. p16+ of p16−). The number of tumor-infiltrating macrophages (CD14+CD163+ and CD14+CD204+) correlated with engraftment success. **$p < 0.01$ p16+ tumors vs. p16− tumors; Mann Whitney *U* test. **B** Representative images showing PD-L1+ tumor and immune cells as well as infiltrating CD8+ cells in primary tumors. Tumor resection specimens were stained with the appropriate antibodies as stated in material & methods. The combined positive score (CPS) was calculated considering PD-L1 positivity in tumor and tumor-infiltrating immune cells. Additional information on engraftment success is given in the lower part (PDX – patient derived xenograft)

Discussion

Patient-derived xenografts (PDX) maintain morphology and molecular profiling of the original tumors, thus providing a platform for the examination of disease biology, biomarkers, and novel therapeutic agents. However, restricted availability of tumour samples hindered the widespread use of PDX. In line with previous research on different cancer entities [7, 10, 27–29], we hypothesized

HNSCC...

Gene	01 Patient PDX	02 Patient PDX	06 Patient PDX	16 Patient PDX	24 Patient PDX	13II Patient PDX	17 Patient PDX	21 Patient PDX	26 Patient PDX	28 Patient PDX	40III Patient PDX	42 Patient PDX	46 Patient PDX
EGFR	p.T790M 52.6% 55.4%	p.T790M 30.5% / wt	synonymous	wt	wt	wt	wt	wt	wt	wt	wt	wt	wt
FGFR3	synonymous	synonymous	synonymous	wt	wt	wt	wt	wt	wt	wt	wt	wt	wt
HRAS	benign, VUS	benign, VUS	p.Gln61Arg 27.6% 50%	wt	wt	wt	wt	wt	wt	wt	wt	wt	wt
KDR	wt	wt	wt	p.Gln472His 65.9% 100.0%	wt	wt	wt	p.Gln472His 100.0%	p.Gln472His 100.0%	p.Gln472His 100.0%	wt	wt	p.Gln472His 100.0%
KIT	wt	wt	wt	wt	wt	p.M537L 48.8% 48.2%	p.M537L 53.7% 66.0%	wt	wt	wt	wt	wt	wt
KRAS	wt / p.D38D 32.7%	wt / p.D38D 7.3%	wt	wt	wt	wt	wt	wt	wt	wt	wt	wt	wt
PIK3CA	wt	p.Glu545Lys 9.0% 13.8%		wt	wt	wt	benign, VUS	wt	wt	wt	wt	wt	wt
SMAD4	p.T197S 56.1% 99.0%	wt	wt	wt	wt	wt	wt	wt	wt	wt	wt	wt	wt
SMARCB1	wt	wt / 5.2%	wt	wt	wt	wt	benign, VUS	wt	wt	wt	wt	wt	wt
TP53	p.Arg282Trp 20.4% 47.7% p.Tyr220Cys 21.7% 48.7%	benign, VUS	benign, VUS	p.R306* 37.0% 100%	benign, VUS		p.Asn200Ilefs 24.9% 99.8%	p.Pro72Arg 100.0%	p.Pro72Arg 100.0%	p.Pro72Arg 100.0% / wt	p.Pro72Arg 100.0% / p.His179Leu 92.6%	M237Ifs2*	p.E294Sfs*51 64.5% 99.3%

Legend: same mutation in patient's tumor and PDX — discrepancy between patient's tumor and PDX — neutral — synonymous variant — benign, VUS — wildtype

Fig. 7 Molecular profile of matched primary tumors and PDX models. Nucleic acids were isolated from snap frozen samples and stored at -80 °C. Purified gDNA samples were than used to detect genomic alterations using the Illumina Cancer Hotspot Panel (Illumina, Berlin, Germany) covering mutations in 50 different genes with an iSeq100 sequencing system (Illumina) according to the manufacturer's protocols. The specific mutations along with the variant allele frequency are depicted in the boxes. Differences between primary patients' samples and matched PDX are highlighted. Mutations were classified in the following categories: non-synonymous—variant is given in the box (in case of the same mutation in the primary and PDX: light blue, difference between primary and PDX: red/blue); synonymous: orange; benign, VUS: light-orange; neutral: grey. The latter is defined as "passenger" mutation that does not play a role in HNSCC; wt – wildtype: light grey. Created with *biorender.com*

that (pre-treatment) endoscopic biopsies contain sufficient viable tumor for PDX growth, in a clinically relevant time frame [21, 30].

Therefore, a comparative analysis on engraftment efficacy of tumor biopsies and surgical specimens was conducted. While both biopsy and surgery specimens were suitable for PDX formation in vivo, the engraftment rate was substantially lower for biopsies.

Recently, PDX engraftment from biopsies has been tested for many cancer entities. The success rates were 3 to 90% using fine- and core needle laparoscopic biopsies [15, 22, 23, 31, 32]. In line with our findings, direct comparisons with surgery sampling showed mainly lower biopsy engraftment rates. For HNSCC, Lilja-Fischer et al. implanted mainly HPV+ oropharyngeal cancer biopsies with a success rate of 33%, which is similar to our biopsy engraftment [24]. In conflict with these results, Kang et al. reported a superior HNSCC biopsy engraftment

of 100% compared to 16% of surgery samples, yet in a very small patient cohort [25]. However, both groups did not specify whether the biopsies were diagnostic tonsillectomies, lymph node metastasis extirpations or endoscopic biopsies. Take rates approaching 100% are more typical for metastatic lymph node biopsies, which are not part of routine HNSCC diagnostics. Reviewing the present results in the scope of previous research, we expect engraftment rates of ~30% for biopsies and 50–70% for surgical specimens in HNSCC. However, comparisons of engraftment rates are impaired by limited standardization: Depending on the authors, the engraftment rate has been reported after one, two or three passages. More differences comprise the mouse strain (complex immunodeficient vs. athymic), the number of animals/tumor and the implantation technique (orthotopic vs. subcutaneous vs. kidney capsule vs. muscle). More standards are highly desirable to reduce laboratory animal expenditure.

A critical factor for engraftment efficacy is tissue ischemia and cryopreservation of tumor samples prior to engraftment that impair viability and thus PDX formation [33–37]. Tissue ischemia has been controlled by pathological diagnostics, processing, and viable freezing within 120 min. Immediate tissue transfer into mice is supposed to enable the highest yield of viable cells, but it also requires a complex infrastructure including timing of surgery, availability of laboratory personnel and accessibility to mice at a specific age (usually < 3 month). We therefore decided to cryopreserve fresh frozen tumor samples prior to engraftment and our engraftment efficacy was comparable to previous research using direct implantation. The standardized cryopreservation enables implantation of several tumor samples simultaneously and re-implantation of frozen backup samples if initial PDX formation fails. Freezing also facilitates reanimation of early passaged tumors at later time points. To date, all individual PDX cases were cryopreserved in P0 and seven have been replanted into NSG mice. All of them grew successfully in P1.

Additional to the higher engraftment rate, surgery samples showed an accelerated in vivo growth. After tumor formation, the growth kinetics was the same in both groups. Handling time, specimen size, p16 status, Ki-67 index, patients' clinical characteristics and implantation ($3 \times 3 \times 3$ mm^3 fragments) did not differ between the study groups. As sampling quality does not appear to be the primary reason, it can only be speculated on the underlying causes for impaired biopsy engraftment. One plausible explanation may be sampling of less proliferating tumor cells in biopsies because of intratumoral heterogeneity [32]. Likewise, the tumor microenvironment at the invasive margin may have played a role, too. Biopsies are usually taken from exophytic tumor areas to avoid bleeding and tumor cell dispersion: These areas are exposed to air, toxins and microorganisms. Also, basal proliferating areas remain untouched. In contrast, PDX of surgical specimens originate from central areas of the tumor to ensure safe pathological margin diagnostics. If the surgery samples are large and margins safe (e.g. laryngectomy) (I) viable cells from the cancer invasion front may be selected and (II) specific areas (center vs. margin) of the tumor may be punched to consider heterogeneity.

To improve engraftment rates, orthotopic implantation of HNSCC biopsy pieces might provide a good alternative. Also, metastasis and accurate mimicry of the original tumors' environment can be anticipated. Another way to increase the number of PDX models from biopsies is a preselection of the tumor type (e.g. focusing only on highly malignant/aggressive cases) or ex vivo enrichment of tumor cells via tumor-surface antigen-based sorting/separation (such as EpCAM or cancer-initiating/stem cells), followed by co-implantation with non-malignant stromal cells. Finally, grafting of three-dimensional patient-derived tumor organoids or even circulating tumor cells is increasingly applied in preclinical research and may help to ameliorate success rates prospectively [38].

Even though surgery samples have many advantages, including non-resectable advanced cancer biopsy samples in preclinical models is crucial. Since these tumors are usually treated by radiation or chemotherapy, drug response prediction would be highly desirable. Additionally, 75% of the p16$^+$ PDX originated from biopsies in this study. HPV-related HNSCC PDX underline the importance of biopsy xenografting in cancer entities, which are mostly treated by irradiation therapy. Improvement of biopsy engraftment could also enable repetitive PDX generation from pre-therapeutic endoscopy, surgery, post-radiation endoscopy and cancer recurrence to study cancer progression and clonal selection.

Previous studies described an association of clinical and pathological features between tumors with rapid and slow PDX growth. In pancreatic cancer, for instance, rapid growth was significantly associated with male gender and lymph node metastases [21]. Likewise, rapid PDX growth was associated with a poor outcome in melanoma and HNSCC patients [10, 30]. A recent study described an association of tumor mutational burden and reduced E7/p16^{INK4A} levels with p16$^+$ HNSCC PDX and organoid engraftment [27]. Hence, successful and rapid PDX establishment is suspected to be predictive for increased risk of recurrence and poor outcome. Since the biobank has been established recently, survival rates could not be calculated. However, previous data on the correlation of PDX engraftment and patient outcome can be confirmed at least partially: One PDX was established from a chemoradiation refractory patient (HNSCC48) who deceased shortly after salvage surgery. This PDX grew rapidly and growth accelerated after serial passaging.

Another important factor in HNSCC research is the tumor microenvironment, since HNSCC naturally shows high immune cell infiltration. Fuji et al., described the impact of the tumor microenvironment on engraftment efficacy of colorectal cancer specimens and concluded that tumor-infiltrating lymphocytes can inhibit engraftment by exerting suppressive effects on tumor growth [39]. The tumor microenvironment was scanned with immunohistochemistry and flow cytometry in the present work. Both methods confirmed increased immune activity in p16$^+$ tumors as part of the immune response to the viral infection compared to p16$^-$ tumors. Regarding the influence of the TME on PDX growth, immunohistochemistry revealed that low CPS scores were associated

with high engraftment rates. Flow cytometric TME analysis identified (tumor associated) $CD14^+CD163^+$ and $CD14^+CD204^+$ macrophages as critical determinants for PDX propagation. Both subtypes are strongly associated with the M2-like phenotype. In breast and lung cancer, circulating $CD14^+CD204^+$ cells are representative for an advanced tumor stage and contribute to metastasis [40, 41]. In esophageal cancer, the high infiltration of $CD163^+$ macrophages is significantly associated with chemoresistance [42]. Because of the value of tumor microenvironment analysis for PDX engraftment and biomarker identification, flow cytometry could become a method of choice for quantitative examination of the immune infiltration. Flow cytometry is timesaving and measures multiple cell types simultaneously in small tumor samples (compared with immunohistochemistry). A major constraint of flow cytometric tumor microenvironment phenotyping is the lack of spatially resolved measurements regarding leukocyte localization within the tumor and its interaction with different cell types, such as tumor cells and cancer-associated fibroblasts. A very recent study integrated histomorphological patterns of immune cell infiltration and mRNA expression data of immune genes in HNSCC. In this study, the status of tumor-infiltrating lymphocytes in the intra-epithelial and stromal compartment was identified as non-redundant biomarker in HNSCC that should be evaluated separately [43]. In the present study, immunohistochemistry was combined with flow cytometry and it suggests the latter as an important add-on tool for tumor microenvironment analysis in preclinical models.

Finally, this work has several limitations. One major limitation is the partial molecular characterization using the 50 gene comprising Illumina Cancer Hotspot Panel. However, HNSCC is characterized by heterogeneous (epi-)genetic alterations and several comprehensive studies did not find reliable molecular biomarkers for PDX engraftment. As the focus was on the tumor microenvironment; applying flow cytometry and immunohistochemistry could identify macrophages differentiation and PD-L1 immune status as potential biomarkers for PDX engraftment. A second limitation relates to tumor heterogeneity: Implantation, histology and cancer sequencing were performed from one sample. Joining punches from different areas may preserve heterogeneity in future studies. Next, the PDX suffer from a selection bias in favor of advanced cancer. However, most HNSCC cancers are already advanced on diagnosis and most T1/2 lesions are sufficiently treated by transoral surgery. Therefore, advanced disease models are more valuable for preclinical research. Still, the results on implantation of specimens from small biopsies may also enhance research on PDX from early-stage lesions.

This study has implications for HNSCC PDX-based research: We have established and characterized new $p16^+$ and $p16^-$ in vitro and in vivo models from primary, recurrent and metastasized HNSCC. The new PDX represent morphology and molecular alterations of the patients' tumors. Using endoscopic biopsies, this new PDX models comprise advanced disease patients that were not eligible for surgery. In this context, the correlation between PDX growth and clinical outcome could lead to the identification of clinical biomarkers.

Even though the engraftment rate is lower, PDX from biopsies are essential to include aggressive recurrent and metastasized carcinomas -that cannot be treated by surgery- in preclinical research. Since PDX engraftment from biopsies is feasible, routine implantation of endoscopic biopsies should be implemented in HNSCC research projects. As a result, biopsy PDX might play a crucial role in personalized therapy for HNSCC patients in advanced tumor stage.

Conclusion

This study describes the successful establishment of patient-derived xenograft models from head and neck cancers obtained from endoscopic biopsies and surgery resection specimens. Additionally to the higher engraftment efficacy of the latter compared to the former, intra-tumoral M2-like macrophages as well as a low PD-L1 expression on tumor and immune cells were identified as independent positive predictors for engraftment. Vice versa, the p16 status had no impact on engraftment efficacy. Finally, PDX models from both sources were successfully transferred and expanded thus broadening the resources for preclinical drug response analyses.

Supplementary Information

The online version contains supplementary material available at https://doi.org/10.1186/s13046-021-02047-w.

> **Additional file 1: Supplementary Table 1**. Patient characteristics and clinical information

Authors' contributions
DS – recruited patients and participated in study design, performed in vivo experiments, participated in data analysis and manuscript writing; TM, NI – processed tumor material, performed in vivo experiments, isolated nucleic

Strüder *et al. Journal of Experimental & Clinical Cancer Research*   (2021) 40:246

Page 12 of 13

acids, carried out flow cytometry, and participated in data analysis; MK—processed tumor material, performed flow cytometry, and cryopreservation of primary and PDX material; JL, SS – recruited and informed patients; AZ, SZ – performed histopathological examinations and participated in immunohistochemical data analysis; AB – participated in histopathological examinations; BS – performed NGS analysis and data interpretation; BF, RM, CGT, CJ – critically revised the manuscript; CM—conceived of the study, performed in vivo experiments, analyzed data, performed statistical analysis, and wrote the manuscript. All authors read and approved the final manuscript.

Availability of data and materials
All data generated or analyzed during this study are included in this published article [and its supplementary information files].

Declarations

Ethics approval and consent to participate
All procedures performed in studies involving human participants were in accordance with the ethical standards of the institutional and/or national research committee and with the 1964 Helsinki declaration and its later amendments or comparable ethical standards. Informed consent was obtained from all individual participants involved in the study. Written informed consent was obtained according to the local Ethics Committee (reference number A2018-0003).
All animal experiments were approved by the local governmental authority (approval number: 7221.3-1-066/18), in accordance with the governmental animal protection law and the EU Guideline 2010/63/EU. All applicable international, national, and/or institutional guidelines for the care and use of animals were followed.

Consent for publication
Not applicable.

Competing interests
The authors declare that they have no competing interests.

Author details
[1]Department of Otorhinolaryngology, Head and Neck Surgery "Otto Koerner", Rostock University Medical Center, Rostock, Germany. [2]Department of Internal Medicine, Medical Clinic III - Hematology, Oncology, Palliative Medicine, Rostock University Medical Center, Schillingallee 70, 18057 Rostock, Germany. [3]Department of Oral and Maxillofacial Surgery, Facial Plastic Surgery, Rostock University Medical Center, Rostock, Germany. [4]Institute of Pathology, Rostock University Medical Center, Rostock, Germany.

References
1. Malone E, Siu LL. Precision medicine in head and neck cancer: myth or reality? Clin Med Insights Oncol. 2018;12:117955491877958. https://doi.org/10.1177/1179554918779581.
2. Guo T, Califano JA. Molecular biology and immunology of head & neck cancer. Surg Oncol Clin N Am. 2015;24(3):397–407. https://doi.org/10.1016/j.soc.2015.03.002.
3. Specenier P, Vermorken JB. Optimizing treatments for recurrent or metastatic head and neck squamous cell carcinoma. Expert Rev Anticancer Ther. 2018;18(9):901–15. https://doi.org/10.1080/14737140.2018.1493925.
4. Dang RP, Le VH, Miles BA, et al. Clinical outcomes in patients with recurrent or metastatic human papilloma virus-positive head and neck cancer. Anticancer Res. 2016;36(4):1703–9.
5. Billard-Sandu C, Tao YG, Sablin MP, Dumitrescu G, Billard D, Deutsch E. CDK4/6 inhibitors in P16/HPV16-negative squamous cell carcinoma of the head and neck. Eur Arch Oto-Rhino-Laryngol. 2020;277(5):1273–80. https://doi.org/10.1007/s00405-020-05891-2.
6. Ordonez R, Otero A, Jerez I, Medina JA, Lupianez-Perez Y, Gomez-Millan J. Role of radiotherapy in the treatment of metastatic head and neck cancer. Onco Targets Ther. 2019;12:677–83. https://doi.org/10.2147/OTT.S181697.
7. Lai Y, Wei X, Lin S, Qin L, Cheng L, Li P. Current status and perspectives of patient-derived xenograft models in cancer research. J Hematol Oncol. 2017;10(1):106. https://doi.org/10.1186/s13045-017-0470-7.
8. Peng S, Creighton CJ, Zhang Y, et al. Tumor grafts derived from patients with head and neck squamous carcinoma authentically maintain the molecular and histologic characteristics of human cancers. J Transl Med. 2013;11:198. https://doi.org/10.1186/1479-5876-11-198.
9. Byrne AT, Alférez DG, Amant F, et al. Interrogating open issues in cancer precision medicine with patient-derived xenografts. Nat Rev Cancer. 2017;17(4):254–68. https://doi.org/10.1038/nrc.2016.140.
10. Karamboulas C, Bruce JP, Hope AJ, et al. Patient-derived xenografts for prognostication and personalized treatment for head and neck squamous cell carcinoma. Cell Rep. 2018;25(5):1318-1331.e4. https://doi.org/10.1016/j.celrep.2018.10.004.
11. Byrne AT, Alférez DG, Amant F, et al. Interrogating open issues in cancer precision medicine with patient-derived xenografts. Nat Rev Cancer. 2017;17(4):254–68. https://doi.org/10.1038/nrc.2016.140.
12. Woo XY, Giordano J, Srivastava A, et al. Conservation of copy number profiles during engraftment and passaging of patient-derived cancer xenografts. Nat Genet. 2021;53(1):86–99. https://doi.org/10.1038/s41588-020-00750-6.
13. Lipner MB, Marayati R, Deng Y, et al. Metformin treatment does not inhibit growth of pancreatic cancer patient-derived xenografts. PLoS ONE. 2016;11(1): e0147113. https://doi.org/10.1371/journal.pone.0147113.
14. Kita K, Fukuda K, Takahashi H, et al. Patient-derived xenograft models of non-small cell lung cancer for evaluating targeted drug sensitivity and resistance. Cancer Sci. 2019;110(10):3215–24. https://doi.org/10.1111/cas.14171.
15 Choi S II, Jeon AR, Kim MK, et al. Development of patient-derived preclinical platform for metastatic pancreatic cancer: pdox and a subsequent organoid model system using percutaneous biopsy samples. Front Oncol. 2019;9:875. https://doi.org/10.3389/fonc.2019.00875.
16. Lee HW, Lee J II, Lee SJ, et al. Patient-derived xenografts from non-small cell lung cancer brain metastases are valuable translational platforms for the development of personalized targeted therapy. Clin Cancer Res. 2015;21(5):1172–82. https://doi.org/10.1158/1078-0432.CCR-14-1589.
17. Kang HN, Choi JW, Shim HS, et al. Establishment of a platform of non-small-cell lung cancer patient-derived xenografts with clinical and genomic annotation. Lung Cancer. 2018;124:168–78. https://doi.org/10.1016/j.lungcan.2018.08.008.
18. Moro M, Bertolini G, Tortoreto M, Pastorino U, Sozzi G, Roz L. Patient-derived xenografts of non small cell lung cancer: resurgence of an old model for investigation of modern concepts of tailored therapy and cancer stem cells. J Biomed Biotechnol. 2012;2012: 568567. https://doi.org/10.1155/2012/568567.
19. Ilie M, Nunes M, Blot L, et al. Setting up a wide panel of patient-derived tumor xenografts of non-small cell lung cancer by improving the pre-analytical steps. Cancer Med. 2015;4(2):201–11. https://doi.org/10.1002/cam4.357.
20. Brown KM, Xue A, Mittal A, Samra JS, Smith R, Hugh TJ. Patient-derived xenograft models of colorectal cancer in preclinical research: a systematic review. Oncotarget. 2016;7(40):66212–25. https://doi.org/10.18632/oncotarget.11184.
21 Pergolini I, Morales-Oyarvide V, Mino-Kenudson M, et al. Tumor engraftment in patient-derived xenografts of pancreatic ductal adenocarcinoma is associated with adverse clinicopathological features and poor survival. PLoS One. 2017;12(8):e0182855. https://doi.org/10.1371/journal.pone.0182855.
22. Hermans E, Van der Merwe SW, Depreeuw J, et al. Successful application of endoscopic ultrasound-guided fine needle biopsy to establish pancreatic patient-derived tumor xenografts: a pilot study. Endoscopy. 2016;48(11):1016–22. https://doi.org/10.1055/s-0042-113597.
23. Wang Z, Fu S, Zhao J, et al. Transbronchoscopic patient biopsy-derived xenografts as a preclinical model to explore chemorefractory-associated pathways and biomarkers for small-cell lung cancer. Cancer Lett. 2019;440–441:180–8. https://doi.org/10.1016/j.canlet.2018.10.014.

24. Lilja-Fischer JK, Ulhøi BP, Alsner J, et al. Characterization and radiosensitivity of HPV-related oropharyngeal squamous cell carcinoma patient-derived xenografts. Acta Oncol. 2019;58(10):1489–94. https://doi.org/10.1080/0284186X.2019.1660802.

25. Kang HN, Kim JH, Park AY, et al. Establishment and characterization of patient-derived xenografts as paraclinical models for head and neck cancer. BMC Cancer. 2020;20(1):316. https://doi.org/10.1186/s12885-020-06786-5.

26. Kang HN, Kim JH, Park AY, et al. Establishment and characterization of patient-derived xenografts as paraclinical models for head and neck cancer. BMC Cancer. 2020;20(1):1–12. https://doi.org/10.1186/s12885-020-06786-5.

27. Facompre ND, Rajagopalan P, Sahu V, et al. Identifying predictors of <scp>HPV</scp> -related head and neck squamous cell carcinoma progression and survival through patient-derived models. Int J Cancer. 2020;147(11):3236–49. https://doi.org/10.1002/ijc.33125.

28. Kimple RJ, Harari PM, Torres AD, et al. Development and characterization of HPV-positive and HPV-negative head and neck squamous cell carcinoma tumorgrafts. Clin Cancer Res. 2013;19(4):855–64. https://doi.org/10.1158/1078-0432.CCR-12-2746.

29. Klinghammer K, Raguse J-D, Plath T, et al. A comprehensively characterized large panel of head and neck cancer patient-derived xenografts identifies the mTOR inhibitor everolimus as potential new treatment option. Int J cancer. 2015;136(12):2940–8. https://doi.org/10.1002/ijc.29344.

30. Ny L, Rizzo LY, Belgrano V, et al. Supporting clinical decision making in advanced melanoma by preclinical testing in personalized immune-humanized xenograft mouse models. Ann Oncol. 2020. https://doi.org/10.1016/j.annonc.2019.11.002.

31. Dong Y, Manley BJ, Becerra MF, et al. Tumor xenografts of human clear cell renal cell carcinoma but not corresponding cell lines recapitulate clinical response to sunitinib: feasibility of using biopsy samples. Eur Urol Focus. 2017;3(6):590–8. https://doi.org/10.1016/j.euf.2016.08.005.

32. Roife D, Kang Y, Wang L, et al. Generation of patient-derived xenografts from fine needle aspirates or core needle biopsy. Surgery. 2017;161(5):1246–54. https://doi.org/10.1016/j.surg.2016.11.020.

33. Linnebacher M, Maletzki C, Ostwald C, et al. Cryopreservation of human colorectal carcinomas prior to xenografting. BMC Cancer. 2010;10:362. https://doi.org/10.1186/1471-2407-10-362.

34. Tanaka R, Kageyama K, Kimura K, et al. Establishment of a liver transplant patient-derived tumor xenograft (PDX) model using cryopreserved pancreatic ductal adenocarcinoma. Anticancer Res. 2020;40(5):2637–44. https://doi.org/10.21873/anticanres.14234.

35. Hernandez MC, Yang L, Leiting JL, et al. Successful secondary engraftment of pancreatic ductal adenocarcinoma and cholangiocarcinoma patient-derived xenografts after previous failed primary engraftment. Transl Oncol. 2019;12(1):69–75. https://doi.org/10.1016/j.tranon.2018.09.008.

36 Guerrera F, Tabbo F, Bessone L, et al. The influence of tissue ischemia time on RNA integrity and patient-derived xenografts (PDX) engraftment rate in a non-small cell lung cancer (NSCLC) Biobank. PLoS One. 2016;11(1):0145100. https://doi.org/10.1371/journal.pone.0145100.

37. Jiang W, Xie S, Liu Y, Zou S, Zhu X. The application of patient-derived xenograft models in gynecologic cancers. J Cancer. 2020;11(18):5478–89. https://doi.org/10.7150/jca.46145.

38 Cho S-Y. Patient-derived xenografts as compatible models for precision oncology. Lab Anim Res. 2020;36(1):14. https://doi.org/10.1186/s42826-020-00045-1.

39. Fujii E, Kato A, Chen YJ, Matsubara K, Ohnishi Y, Suzuki M. The status of donor cancer tissues affects the fate of patient-derived colorectal cancer xenografts in NOG mice. Exp Anim. 2015;64(2):181–90. https://doi.org/10.1538/expanim.14-0080.

40. Maeda R, Ishii G, Neri S, et al. Circulating CD14+CD204+ cells predict postoperative recurrence in non-small-cell lung cancer patients. J Thorac Oncol. 2014. https://doi.org/10.1097/JTO.0000000000000044.

41. Zhang B, Cao M, He Y, et al. Increased circulating M2-like monocytes in patients with breast cancer. Tumor Biol. 2017;39(6):1010428317711571. https://doi.org/10.1177/1010428317711571.

42. Yamamoto K, Makino T, Sato E, et al. Tumor-infiltrating M2 macrophage in pretreatment biopsy sample predicts response to chemotherapy and survival in esophageal cancer. Cancer Sci. 2020;111(4):1103–12. https://doi.org/10.1111/cas.14328.

43. Badr M, Jöhrens K, Allgäuer M, et al. Morphomolecular analysis of the immune tumor microenvironment in human head and neck cancer. Cancer Immunol Immunother. 2019;68(9):1443–54. https://doi.org/10.1007/s00262-019-02378-w.

Publisher's Note